7 Shallow Lava Theory

N.J. Balmforth[1], A.S. Burbidge[2], and R.V. Craster[3]

[1] Department of Applied Mathematics and Statistics, School of Engineering, University of California at Santa Cruz, CA 95064, USA
[2] School of Chemical Engineering, University of Birmingham, Edgbaston, Birmingham, B15 2TT, U.K.
[3] Department of Mathematics, Imperial College of Science, Technology and Medicine, London, SW7 2BZ, UK

7.1 Introduction

In Chap. 2, we mentioned that lava was a non-Newtonian fluid, and discussed a variety of state-of-the-art constitutive laws that crudely model some of the properties of such fluids. In the current chapter, we go further in this direction and describe more developments of a theoretical model for lava flows. Lava flows have recently been the subject of a review by Griffiths [1] (see also Chap. 6). Our aim here is to illustrate the use of viscoplastic rheological models in this problem.

Viscoplastic fluid models are appropriate because silicic lava contains large quantities of silicate crystals that provide a significant yield stress and crystallize with temperature to produce highly temperature-dependent material properties. Many lava formations are built from this material. For example, silicic lava forms the bulk of the lava domes that emerged after eruptions on Katmai and Mount St. Helens, and which are shown in Figs. 7.1 and 7.2. These structures were gradually built up by the slow effusion of lava from a smaller vent. Other lava flows contain less silicates, such as the basaltic lavas of Mount Etna and Hawaii. These lavas generally have both a smaller yield stress and viscosity, with the result that they flow much more easily and create morphology more like that of rivers, see Fig. 7.3.

Although we have models from non-Newtonian fluid mechanics at our disposal for roughly describing some of the rheology of lava, it is still a formidable task to solve the resulting governing equations – we have a non-isothermal, three-dimensional evolving fluid flow with a free surface and strongly varying material properties. Though this does not rule out full-scale numerical simulation as an option, it does mean that such an approach is far from straightforward. Moreover, because we do not completely understand all the input physics, one can justifiably question the usefulness of embarking on such a difficult exercise. Fortunately, lava flows are often relatively shallow, and as in other fields of geophysical fluid dynamics, one is tempted to exploit this attribute to build simpler theoretical models describing the phenomena. The construction amounts to an asymptotic expansion of the governing equations, and furnishes a "shallow-lava theory." This is entirely analogous to theories developed for avalanches, ice, mud

N.J. Balmforth and A. Provenzale (Eds.): LNP 582, pp. 164–187, 2001.

Fig. 7.1. The Novarupta dome that formed after the 1912 Katmai eruption in Alaska; the dome has diameter 800 ft and is 200 ft high. This photograph is courtesy of the USGS/Cascades Volcano Observatory and further details regarding this dome and others can be found at http://vulcan.wr.usgs.gov/home.html

Fig. 7.2. The lava dome inside the crater of Mount St. Helens. Photographs courtesy of USGS

and debris flows, as described in other chapters in this volume. Here we describe elements of a shallow-lava theory.

Theoretical modelling of this kind can be complemented by laboratory experiments: extrusions in the laboratory with fluids that act as analogues of lava provide a controllable visualization of the important fluid mechanics. The most commonly used analogue fluids for isothermal flows are kaolin–water slurries [2,3], which, as we saw in earlier chapters, are approximately Herschel–Bulkley fluids. Later in this chapter we describe some experiments with such slurries. These experiments nicely demonstrate some of the fluid dynamical effects present in lava flows and which can be understood with the theory. Moreover, detailed comparisons verify that, in the simpler isothermal limit, the theory compares quantitatively with laboratory analogues. Non-isothermal experiments have also been conducted using wax, syrup and slurries of wax and kaolin [4,5,6] – as de-

Fig. 7.3. Two Hawaiian lava flows. Photographs courtesy of USGS

scribed in Chap. 6, these experiments have many common morphological features with real lava formations.

We open our discussion with the derivation of the shallow-lava theory for axisymmetrical, cooling lava domes. Our main aim is to summarize the equations that one needs to solve for cooling domes; this theory is also relevant in some entirely different subjects, such as spreading non-isothermal fluids in chemical engineering [7]. But when we deal with explicit solutions and experimental comparisons, we retire to the simpler isothermal limit. After discussing isothermal domes, we switch problems and turn to isothermal lava flows on slopes. The mathematical formulation is much the same, and we focus on a specific geological issue – the creation of "levees" bordering downslope flows.

7.2 Mathematical Formulation

7.2.1 Governing Equations in Axisymmetrical Geometry

Our vision of the problem (Fig. 7.4) is one in which there is a vent centred at the origin of a cylindrical polar coordinate system (r, θ, z). The material (lava or analogue fluid) is extruded through the vent and then spreads out laterally over a horizontal plate located on the plane $z = 0$. Assuming axisymmetry and

incompressibility, the governing equations consist of conservation of momentum,

$$\rho\left(u_t + uu_r + wu_z\right) = -p_r + \partial_r\tau_{rr} + \partial_z\tau_{rz} + \frac{1}{r}\tau_{rr} \tag{7.1}$$

and

$$\rho\left(w_t + uw_r + ww_z\right) = -p_z - \rho g + \partial_r\tau_{zr} + \partial_z\tau_{zz} + \frac{1}{r}\tau_{rz}\ , \tag{7.2}$$

continuity,

$$\frac{1}{r}\partial_r(ru) + w_z = 0\ , \tag{7.3}$$

and the heat equation,

$$\rho c_p\left(T_t + uT_r + wT_z\right) = \frac{1}{2}\tau_{ij}\dot{\gamma}_{ij} + \mathcal{K}\left[\frac{1}{r}\partial_r(rT_r) + T_{zz}\right] + \mathcal{S}\ . \tag{7.4}$$

In these equations, the fluid motions are described by the velocity field $(u, 0, w)$, the pressure p, density ρ, and temperature T. Also, g is gravity, c_p is specific heat, $\mathcal{K}$ is the thermal conductivity, and $\mathcal{S}$ denotes any latent heat release on solidification or crystallization in the material. The subscripts (r, z) denote partial derivatives, except in the case of the stress components, τ_{ij}, and then we use the notation ∂_r, and so on. The material variables, c_p, ρ and $\mathcal{K}$, could, in principle, be temperature dependent, but for simplicity we treat them as constants.

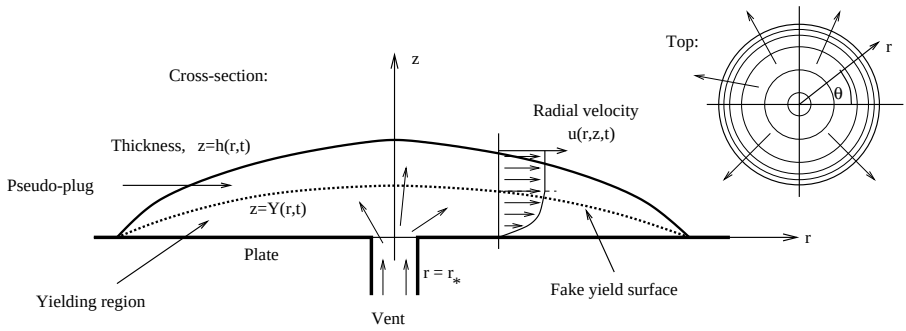

Fig. 7.4. Sketch of an expanding dome

For the cooling problem of interest here, the main source of latent heat release is through a gradual process of crystallization: Lava is a cocktail of different minerals, each crystallizing at a temperature that depends upon the composition. As a result, lava solidifies not at a single temperature, but over a range bounded by the "liquidus" and "solidus" temperatures (where the material is completely fluid and a crystalline solid respectively). The crystal content (expressed as a volumetric fraction, ϕ) varies throughout this range, and the resulting fluid structure can be very complex. Here, we ignore the complicated physical details of

the solidification process and opt for a simple model in which the crystal content is a known function of the temperature alone: $\phi = \phi(T)$. Then,

$$\mathcal{S} = \rho\mathcal{L}(\phi_t + u\phi_r + w\phi_z) \equiv \rho\mathcal{L}\phi_T(T_t + uT_r + wT_z) \,, \tag{7.5}$$

where $\mathcal{L}$ is the latent heat of crystallization and $\phi_T = \mathrm{d}\phi/\mathrm{d}T$.

As discussed in Chap. 2, we adopt the Herschel–Bulkley model for the rheology of the fluid:

$$\tau_{ij} = \left(K\dot\gamma^{n-1} + \frac{\tau_p}{\dot\gamma}\right)\dot\gamma_{ij} \qquad \text{for } \tau \geq \tau_p \tag{7.6}$$

and

$$\dot\gamma_{ij} = 0 \qquad \text{for } \tau < \tau_p \,, \tag{7.7}$$

where τ_p is the yield stress, K is the consistency and n the power-law parameter. Also required are the second invariants of the stress and strain rate:

$$\tau = \sqrt{\tau_{ij}\tau_{ij}/2} \,, \quad \dot\gamma = \sqrt{\dot\gamma_{ij}\dot\gamma_{ij}/2} \,. \tag{7.8}$$

We allow for the temperature and crystal dependence of the material by allowing the consistency and yield stress to vary: $K \to K(\phi, T)$ and $\tau_p \to \tau_p(\phi, T)$. We leave the precise dependences arbitrary, but sensible choices include the Arrhenius law and the Einstein–Roscoe relation (Chap. 2). To derive a thin layer model, we prescribe $K(\phi_a, T_a) = K_*$ and $\tau_p(\phi_a, T_a) = \tau_{p*}$ as the values evaluated at the crystal content, ϕ_a, and temperature, T_a, relevant to the ambient conditions.

7.2.2 Boundary Conditions for Cooling, Expanding Domes

On the plate beneath the fluid ($z = 0$), we impose no-slip on the velocity field. At the vent, we must modify this condition to account for the extrusion. This leads to the boundary conditions,

$$u = 0 \quad \text{and} \quad w = w_s(r, t) \quad \text{on } z = 0 \,, \tag{7.9}$$

where $w_s(r, t)$ is the vertical velocity of material exiting the vent. For simplicity, we also prescribe the heat flux on $z = 0$:

$$\mathcal{K}T_z = \rho(c_p - \phi_T\mathcal{L})(T - T_e)w_s \qquad \text{on } z = 0 \,, \tag{7.10}$$

where T_e is the "eruption" temperature. This means that the plate is insulating away from the vent, but the arrival of hot fluid generates an incoming heat flux.

The surface of the dome, $z = h(r, t)$, is stress-free, and so

$$h_t + uh_r = w \tag{7.11}$$

and

$$\begin{pmatrix} \tau_{rr} - p & \tau_{rz} \\ \tau_{zr} & \tau_{zz} - p \end{pmatrix}_{z=h} \begin{pmatrix} -h_r \\ 1 \end{pmatrix} = \begin{pmatrix} 0 \\ 0 \end{pmatrix} \,. \tag{7.12}$$

The thermal boundary condition incorporates surface cooling:

$$\mathcal{K}\mathbf{n}\cdot\nabla T = -F(T)\ , \tag{7.13}$$

where $\mathbf{n}$ is the outward pointing normal. Various forms are possible for $F(T)$, depending on the specific physical conditions. The simplest model is Newton's law of cooling: $F(T) = a(T - T_a)$, where a is a constant. For lava, if the dominant heat loss is through thermal radiation, the Stefan–Boltzmann black-body law is appropriate, although forced convection of heat by wind can also be appreciable [8]. For the experimental slurries, domes are cooled by both conduction and convection in overlying water, each characterized by some functional form for $F(T)$ [6].

7.2.3 Thin-layer Theory

The full governing equations compose a system of coupled partial differential equations with an evolving free boundary. One could embark upon a heavy numerical simulation using, for example, finite element calculations. However, given the relatively thin profiles of lava domes we are also primed for an asymptotic reduction using thin-layer theory. The aim of the theory is to reduce the complexity of the equations, whilst still retaining the most important physics.

To perform the analysis, it is first expedient to non-dimensionalize the equations as follows: we take H, a characteristic thickness of the fluid layer, as the dimension of the vertical coordinate, and L as a horizontal length-scale. We measure the velocities, u and w, by V and HV/L respectively, and time by L/V. Then we set

$$r = L\tilde{r}\ , \quad z = H\tilde{z}\ , \quad u = V\tilde{u}\ , \quad w = (VH/L)\tilde{w}\ , \tag{7.14}$$

$$t = (L/V)\tilde{t} \quad h = H\tilde{h} \quad \text{and} \quad p = \rho g H\ \tilde{p}\ ; \tag{7.15}$$

the tilde decoration denotes the non-dimensional variables. The temperature field is non-dimensionalized using the temperature drop between eruption and ambient temperature:

$$T = T_a + (T_e - T_a)\Theta \equiv T_a + \Delta T\Theta\ . \tag{7.16}$$

Now, given our non-dimensional units, we may measure the stresses by the quantity, $\rho g H^2/L$. However, units for the stresses can also be given based on the constants of the constitutive model. As a result, there is a relationship amongst the various units that we may choose to have the form,

$$V^n = \frac{\rho g H^{n+2}}{K_* L}\ . \tag{7.17}$$

This relation also reflects a balance of terms in the momentum equations (the horizontal pressure gradient with the force from the vertical shear stress) which is standard in "lubrication theory".

Thin-layer theory proceeds by introducing the scalings above into the governing equations and then taking the limit, $H/L = \epsilon \to 0$, with a number of non-dimensional numbers held fixed [9]. To leading order, the governing equations become

$$p_r - \partial_z \tau_{rz} = 0 \,, \qquad p_z + 1 = 0 \,, \tag{7.18}$$

$$\frac{1}{r}\partial_r (ru) + w_z = 0 \tag{7.19}$$

and

$$\Theta_t + u\Theta_r + w\Theta_z = \kappa \Theta_{zz} \,, \tag{7.20}$$

where

$$\kappa = \left(1 - \frac{\phi_T \mathcal{L}}{c_p}\right)^{-1} \frac{\mathcal{K} L}{\rho c_p V H^2}$$

is a dimensionless, effective diffusivity (an inverse Peclet number) depending on temperature. The acceleration terms disappear from the momentum equations because the Reynolds number can be taken to be small (the flow is typically laminar), and viscous heating can be ignored for lava and most laboratory analogue fluids (the "Brinkman number" is small). The crucial parameter in the energy equation is κ: If $\kappa \gg 1$, the diffusive term is dominant in the energy equation, and further asymptotic simplification follows [9]. This limit corresponds to rapid heat diffusion, and in the lava literature this is sometimes called the thermally mixed limit. However, for lava and many analogue materials, κ is order one, and heat diffuses relatively slowly. In this circumstance, we are faced with dealing with the heat equation as a partial differential equation at leading order.

The rescaling of the constitutive equation leads to

$$\tau_{rz} = \frac{1}{\dot\gamma}\left[\mathcal{A}(\Theta)\dot\gamma^n + \mathcal{B}(\Theta)\right] u_z \qquad \text{for } \mathcal{B}(\Theta) < \tau \,, \tag{7.21}$$

$$u_z = 0 \quad \text{for } \mathcal{B}(\Theta) > \tau \,, \tag{7.22}$$

where

$$\tau \equiv |\tau_{rz}| \qquad \text{and} \qquad \dot\gamma = |u_z| \,, \tag{7.23}$$

and, given that $\phi = \phi(\Theta)$,

$$\mathcal{A}(\Theta) = \frac{K(\phi, T)}{K_*} \,, \qquad \mathcal{B}(\Theta) = B\frac{\tau_p(\phi, T)}{\tau_{p*}} \qquad \text{and} \qquad B = \frac{\tau_{p*} L}{\rho g H^2} \,. \tag{7.24}$$

The "Bingham number", B, is a dimensionless measure of the yield stress.

The boundary conditions become

$$u = 0 \,, \quad w = w_s \,, \quad \kappa\Theta_z = (\Theta - 1)w_s \qquad \text{on } z = 0 \,, \tag{7.25}$$

and

$$h_t + uh_r = w \,, \qquad \tau_{rz} = p = 0 \,, \qquad \Theta_z = -\alpha\Theta \qquad \text{on } z = h(r,t) \,, \tag{7.26}$$

where α denotes the non-dimensional "cooling law",

$$\alpha(\Theta) = \frac{H}{\mathcal{K}\Delta T} F(T) \ . \tag{7.27}$$

The momentum equations (7.18) can be integrated once:

$$p = h - z \ , \qquad \tau_{rz} = -h_r(h - z) \ , \qquad \tau = (h - z)|h_r| \ . \tag{7.28}$$

The magnitude of the shear stress is measured by τ. This decreases from a maximal value of $\tau(r, z = 0, t) = h|h_r|$ on the base of the fluid, to zero on the stress-free surface. If $h|h_r| < \mathcal{B}[\Theta(r, 0, t)]$, the fluid is not stressed sufficiently to yield anywhere over its depth, and the dome is stationary. But, when $h|h_r| > \mathcal{B}[\Theta(r, 0, t)]$, the fluid near the base of the dome must yield and flow. In this case, because τ decreases with z to zero, there is a surface, $z = Y(r, t)$, on which $\tau = \mathcal{B}$, given by

$$Y(r, t) = h + \frac{\mathcal{B}[\Theta(r, Y, t)]}{h_r} \ . \tag{7.29}$$

Above this surface, the stress apparently fall beneath the yield stress, and so the fluid is predicted to flow like an unyielded, rigid "plug" with $u_z = 0$. This result is surprising given that the dome is expanding – such spreading flows are divergent, and so the fluid cannot be truly rigid. In the past this apparent contradiction has mistakenly led to the belief that lubrication-style analyses of the sort described here are not self-consistent. The mistake is to identify the flow in $z > Y(r, t)$ as a true "plug flow" – a more refined asymptotic analysis shows that this region is actually weakly yielding [10], and sufficiently so to account for the spreading of the dome. A better terminology is to refer to the weakly yielding region as a "pseudo-plug." (One sees this feature also in Chap. 22).

Equations (7.21) and (7.28) can now be combined into

$$u_z = \begin{cases} -h_r^{(1-n)/n}[\mathcal{A}(\Theta)]^{-1/n}(Y - z)^{1/n} h_r & z < Y(r, t) \\ 0 & z \geq Y(r, t) \end{cases} \tag{7.30}$$

(at least to leading order), which means that the flow is approximately parabolic in the lower, yielding region and constant in the pseudo-plug (see the definition sketch in Fig. 7.4).

We next integrate the continuity equation (7.19) in z, using the boundary conditions at the surface and base, to obtain an evolution equation for the height $h(r, t)$:

$$h_t + \frac{1}{r}\partial_r\,(r\mathcal{U}) = w_s \ , \tag{7.31}$$

where

$$\mathcal{U}(r, t) = \int_0^h u \mathrm{d}z = \sigma h^2 |h_r|^{1/n} \int_0^\eta \frac{(1 - \zeta)(\eta - \zeta)^{1/n}}{[\mathcal{A}(\Theta)]^{1/n}} \mathrm{d}\zeta \ , \tag{7.32}$$

with $\sigma = \mathrm{sgn}(h_r)$ and $\eta = Y/h$ ($\zeta \equiv z/h$). Because η depends on temperature, we cannot integrate this equation without solving the energy equation (7.20),

and we cannot evolve that equation without knowing $h(r,t)$ and the velocity field. Thus, our shallow-lava theory now grinds to a halt analytically, leaving a coupled, integro-differential system for $h(r,t)$ and $\Theta(r,z,t)$. Though this system is still rather complicated, it is simpler than the original governing equations.

7.3 Isothermal Domes

7.3.1 Shallow Isothermal Domes

The shallow-lava theory simplifies significantly if the temperature dependence of the fluid drops out of the problem. Such is the case if the fluid did not have time to cool, or cooled to the ambient temperature immediately. Then we may omit the heat equation and set $\mathcal{A} = 1$ and $\mathcal{B} = B$, leaving only a single evolution equation for the height field:

$$h_t + \frac{1}{r}\partial_r\,(r\mathcal{U}) = w_s\ , \qquad \mathcal{U} = -\frac{n\eta h^2(1+2n-n\eta)}{(n+1)(2n+1)}|hh_r\eta|^{1/n}\mathrm{sgn}(h_r)\ , \quad (7.33)$$

where $\eta = \mathrm{Max}(1 - B/|hh_r|, 0)$.

Representative solutions of these equations are shown in Fig. 7.5 for $n = 1$ and an influx given by $w_s = 0.1\ \mathrm{Max}(r_*^2 - r^2, 0)$, where $r_* = 0.15$ is the dimensionless vent radius. We also pre-wet the plate beneath the dome (by taking initial conditions with $h(r,t)$ small but everywhere finite) in order to avoid mathematical complications associated with contact lines at the rim of the dome. Figure 7.5 shows the height and yield surfaces for three values of the Bingham number B. Newtonian-like domes (with $B \ll 1$, as in panel (a)) spread laterally much further than yield-stress-dominated domes (with $B \sim 0.1$ or larger, as in panel (c)); the latter rise to greater heights due to the conspiracy between the viscous and yield stress.[1]

For Newtonian domes ($B = 0$), $\eta = 1$, and one can find a similarity solution to the thin-layer equations for point sources [11]. This solution predicts that $R(t) \sim t^{1/2}$ and $h(0,t) \sim t^0$, which also follow directly from dimensional scaling analysis of the full governing equations [4].

In yield-stress dominated domes, only a thin fluid layer near the base yields. Hence, $\eta \to 0$, giving $h \approx -B/h_r$, and then

$$h = \begin{cases} \sqrt{2B(R-r)} & r < R \\ 0 \quad r > R\,. \end{cases} \quad (7.34)$$

[1] Formally speaking, the thin-layer theory is not valid at the vent, where $h_r \to 0$, and at the rim, where radial gradients become as sharp as vertical ones. The condition $h_r(0,t) = 0$ also leads to the curious behaviour of the apparent yield surfaces in Fig. 7.5 near $r = 0$. Neither problem is especially important to the overall evolution of the dome. A similar difficulty arises in shallow-ice theory, and a later chapter by Hutter is partly motivated by them.

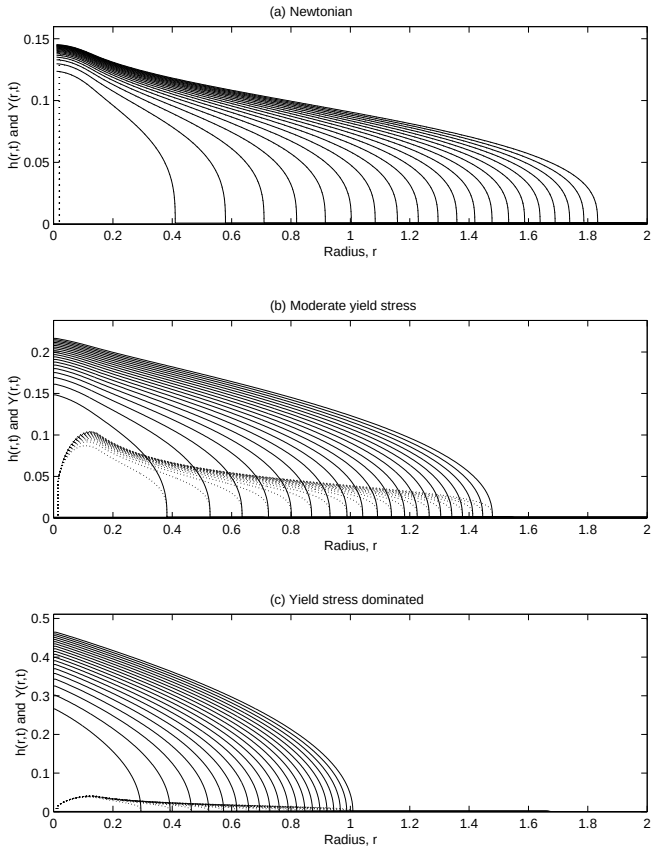

Fig. 7.5. Evolution of the height field, $h(r,t)$, together with the "yield" surface, $Y(r,t)$ (shown by the dotted lines) for various values of B; snapshots of the solution are shown every 500 time units. In panel (**a**), $B = 10^{-5}$ and the dome is effectively Newtonian. For panel (**b**) $B = 0.01$, and the dome in panel (**c**) with $B = 0.1$ is dominated by the yield stress

The time rate of change of the radius, $R(t)$, is dictated by the mass conservation law,

$$\frac{\mathrm{d}}{\mathrm{d}t}\int_0^\infty h(r,t)r\mathrm{d}r = \int_0^\infty w_s(r,t)r\mathrm{d}r\ . \tag{7.35}$$

With a constant inflow rate, Q,

$$R(t) = \frac{1}{(2B)^{1/5}}\left(\frac{15Qt}{8\pi}\right)^{2/5}\ , \qquad h(0,t) = (2BR)^{1/2}\ , \tag{7.36}$$

an asymptotic result also deduced by Nye [12].

7.3.2 Restoring the Dimensions

One convenient test of a theory is how it compares to experiments designed as laboratory analogues. To generate such theoretical comparisons, we must first restore the dimensions in our numerical solutions, thus reversing our earlier non-dimensionalization. To do this we need to estimate the physical length scales, L and H, and the characteristic velocity, V. In the experiments, we fix the vent radius, R_*, and set the extrusion rate, Q. These values can be compared to the dimensional vent radius, $r_*L = 0.15L$, and extrusion rate, $0.05\pi r_*^4 LHV \approx 8\times10^{-5}LHV$, used in the computations. Hence, $L = 1\,\mathrm{cm}$ and $HV = 1.26\times10^6 Q$ (with Q in mks units). We also have the relation (7.17), from which it follows that

$$H = \left(\frac{KL}{\rho g}\right)^{1/(n+2)} \left(1.26\times10^6 Q\right)^{n/(n+2)} \ . \tag{7.37}$$

This allows us to compute H, V and B given ρ, Q and the rheological parameters of the fluid, and thereby reconstruct the dimensional radius, height and time.

7.3.3 Experiments

The experiments have an uncomplicated design consisting of a piston that extrudes a controlled volume flux of slurry onto a horizontal plate. For the domes that then form (which were always axisymmetrical), we record the radius and height above the vent. The slurry is a suspension of kaolin (Dry Branch Kaolin Company) in de-ionized water, and different mixtures of water and kaolin are used in order to vary the rheological parameters. For each mixture, we fit the rheological data using a Herschel–Bulkley model; the rheological properties of the slurries are summarized in Table 2.1 and Fig. 2.2 of Chap. 2. A variety of (time-independent) flow rates, Q, is also used; we quote results for the fastest and slowest of these ($0.18\,\mathrm{cm}^3/\mathrm{s}$ and $0.54\,\mathrm{cm}^3/\mathrm{s}$).

The heights and radii are shown versus time in Fig. 7.6 and 7.7 for kaolin–water slurries mixed in the ratio 0.6:1 and 0.8:1 by weight. The theoretical curves from the shallow lava theory are added for comparison, and are in fair agreement. The dome heights compare least favourably, but this should be tempered by the fact that there were some experimental difficulties in taking this measurement. The figures also show the asymptotic result for large yield stress (Nye's theory), which overestimates the radii and underestimates the heights (Blake [3] uses an empirical correction to account for this error). More paste-like materials with kaolin to water ratios of 1:1 and 1.2:1 were modelled with similar accuracy by the thin-layer theory. Typically these had larger Bingham numbers, ~ 0.19, and were also adequately modelled using Nye's solution.

In Chap. 2 we mentioned that kaolin slurries show some hysteresis in their stress-strain-rate relations, suggesting that the fluid microstructure does not reform in the same way as it is destroyed. In the extrusion experiments, the microstructure disintegrates as the fluid is pushed up the vent, and then reforms as the dome spreads and the stresses gradually decline. This means that the "down-curve" is most suitable for modelling the experiments. We illustrate

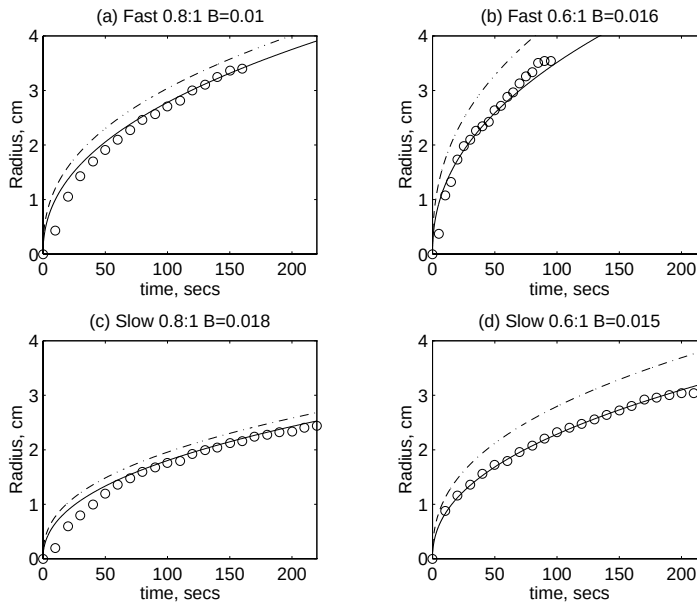

Fig. 7.6. Experimental and theoretical comparisons of dome radii for kaolin–water domes. The solid line gives the result found from shallow lava theory, the circles are the experimental data and the dot-dash line is Nye's result for large B. The values of B are estimated as described in Sect. 7.3.2

the importance of this choice by using another material, Celacol (Courtaulds), also described in Chap. 2, that shows pronounced hysteresis. The comparison between theory and experiment for this material is shown in Fig. 7.8. The two are in agreement only if rheological data from the down curve are used to fit the parameters of the Herschel–Bulkley model; use of the data from the "up-curve" leads to significant disagreement. Evidently, the best model for Celacol would be one accounting for hysteresis, but if we insist on using a model like Herschel–Bulkley we should exercise care in interpreting the rheological data.

7.4 Flows on Inclined Planes

7.4.1 Shallow Flow Dynamics

If the plate beneath the fluid is inclined, the circular symmetry of an expanding dome is broken. Instead, the fluid slumps downslope, leading to elliptical domes for low inclinations, and fully fledged channel flows on larger slopes. We now turn to a theoretical consideration of these structures, again specializing to isothermal conditions.

To generalize the theory it is first helpful to consider a new, Cartesian coordinate system, (x, y, z), in which $z = 0$ again coincides with the base of the

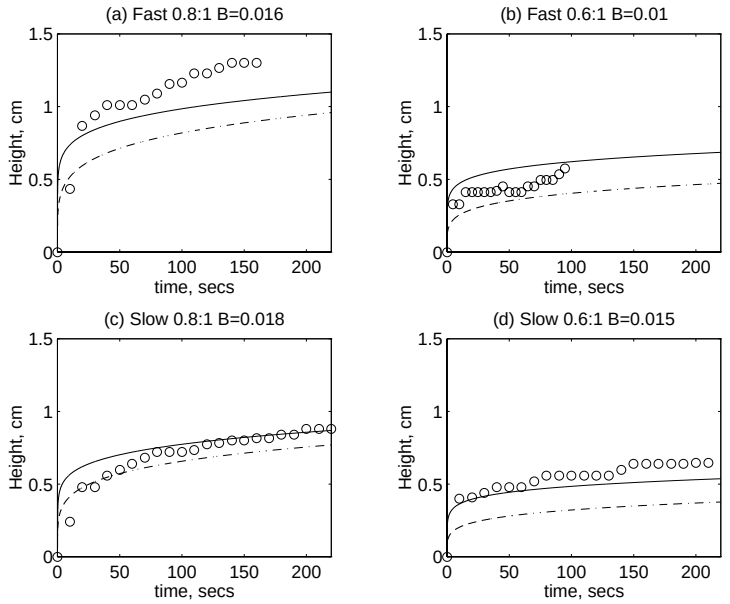

Fig. 7.7. Experimental and theoretical comparison of dome heights for kaolin–water domes. The solid line gives the result found from shallow lava theory, the circles are the experimental data and the dot-dash line is Nye's asymptotic, large B, result

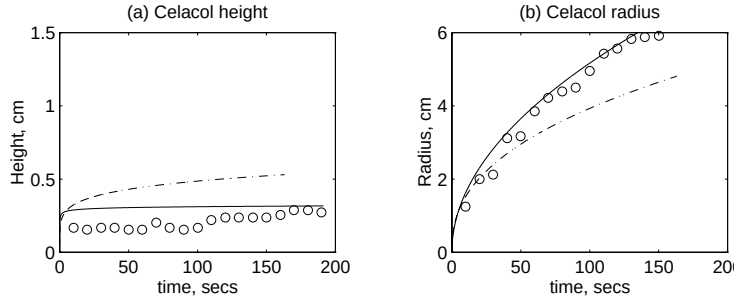

Fig. 7.8. Experimental and theoretical comparison of dome evolution for a Celacol dome. Panel (**a**) shows height measurements and in panel (**b**) we compare radii measurements. The circles show the experimental data. The solid lines are the numerical results using the rheological data from the down curves, and the dash-dotted lines show the corresponding results using the up-curves

fluid, which is now on an inclined plane. As shown in Fig. 7.9, we also take the coordinate x to lie in the downslope direction, and ϕ to be the angle of the plane's inclination from the horizontal. From here we could again write down the governing equations, non-dimensionalize, expand asymptotically, and finally arrive at a relevant thin-layer model [10] (see also Chap. 22). We will not go through the details here, and instead offer some simple arguments that indicate how we should generalize (7.33).

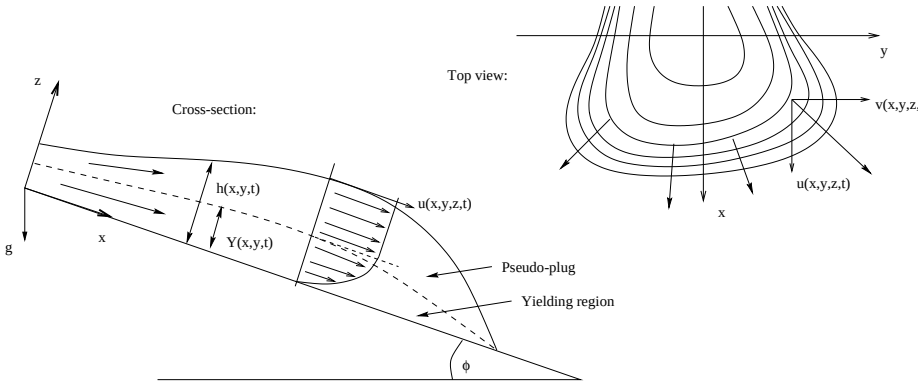

Fig. 7.9. Sketch of a flow on an inclined plane. ϕ is the angle of inclination

The key feature of the thin-fluid dynamics is that thickness variations drive a flow that is down-gradient with respect to the height field: $\mathcal{U} \sim -|h_r|^{1/n-1}h_r$. A natural generalization is therefore to introduce an analogous depth-integrated lateral velocity, $\mathcal{V}$, and take $(\mathcal{U}, \mathcal{V}) \sim -s^{1/n-1}(h_x, h_y)$, where $s = \sqrt{h_x^2 + h_y^2}$ is the mean surface gradient. This naturally accounts for the shape of the fluid, but not the background slope, which also forces flow in the $x-$direction. To take account of the slope we make the replacement $h_x \to h_x - S$, where $S = \epsilon^{-1} \tan\phi$ is a measure of the slope relative to the fluid's typical aspect ratio (assumed to be order one, so that the slope must be sufficiently gentle). Thence, with other dependences as before,

$$h_t + \mathcal{U}_x + \mathcal{V}_y = w_s \ , \qquad \begin{pmatrix} \mathcal{U} \\ \mathcal{V} \end{pmatrix} = \frac{n\eta h^2 (s\eta h)^{1/n}(1 + 2n - n\eta)}{s(n+1)(2n+1)} \begin{pmatrix} S - h_x \\ -h_y \end{pmatrix} \ , \quad (7.38)$$

with

$$\eta = \mathrm{Max}\left(1 - \frac{B}{hs}, 0\right) \qquad \text{and} \qquad s = \sqrt{(S - h_x)^2 + h_y^2} \qquad (7.39)$$

(once again, w_s denotes the extrusion speed above any vents and $Y = h\eta$ is the fake yield surface), which also results from a proper expansion (see Chap. 22).

7.4.2 Inclined Domes

Experiments illustrating how domes slump downhill and lose symmetry are shown in Fig. 7.10. The slurry used in these experiments is a mixture of water and "joint compound" (a commonly available, kaolin-based material). Some more careful experiments with a true kaolin slurry are shown in Chap. 6 and explored further in [15].

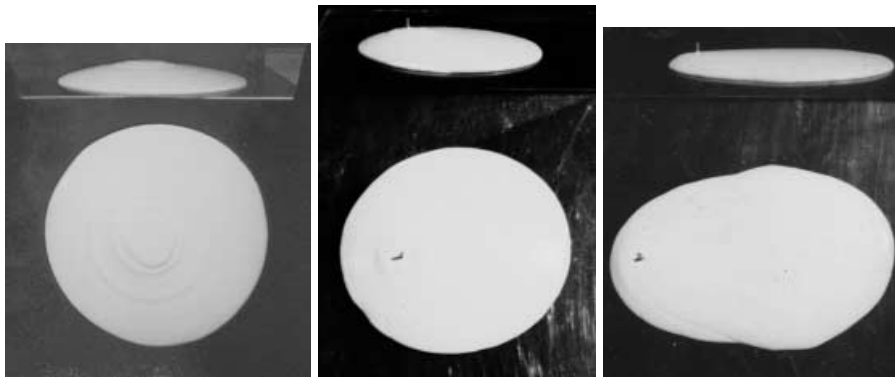

Fig. 7.10. Slumped domes on inclined planes. Shown are domes on slopes with inclinations of roughly 0, 10 and 20 degrees. The slurry, a mixture of water and "joint compound" (a kaolin-based material that is commonly available at hardware shops), is fed onto the plane through a narrow tube from a reservoir held just above. An inclined mirror at the top of each pictures gives a side view of the domes. For the second two domes, a marker indicates the position of the feeder from the reservoir

To compare with experimental images like these we solve the thin-layer equations numerically. As for symmetrical domes we take $w_s = 0.1\ \mathrm{Max}(0.15^2 - r^2, 0)$, and use a numerical scheme: VLUGR2 [16]. One such computation is shown in Fig. 7.11. This shows a dome with $B = 0.01$ and $n = 1$ on a slope with $S = 0.5$. As indicated by the fake yield surfaces, this dome is not far from being Newtonian. The yield stress has most effect upstream of the vent where the fluid becomes almost stationary over longer times. The overall appearance of the dome is similar to the experimental pictures.

When $\eta \to 0$ (large B), and the dome is dominated by yield stress, the thin-layer model simplifies substantially. From the condition, $\eta \approx 0$, we obtain the nonlinear first-order partial differential equation,

$$(S - h_x)^2 + h_y^2 = B^2/h^2 \ . \tag{7.40}$$

This simpler equation determines the structure of domes that are either dominated by the yield-stress, or slump to rest at the termination of an extrusion. We can solve the equation using Charpit's method [14]: First we scale the equations

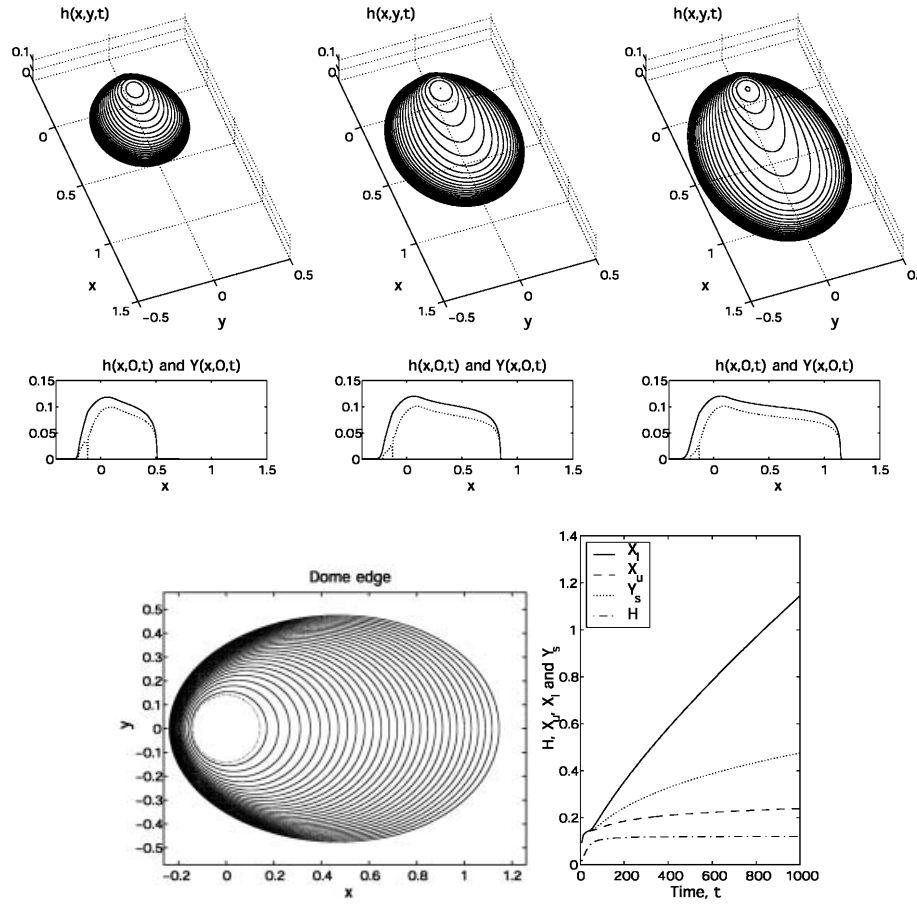

Fig. 7.11. Slumped domes on inclined planes, computed numerically using the thin-layer model. The top row of pictures show three snapshots of the domes at times 333, 666 and 1000. Directly below are the corresponding height profiles and yield surfaces along the midsection ($y = 0$). The lower panels show a sequence of curves showing the dome's edge (the curves show the edge every 6.66 time units), and the evolution of the cross-stream half-thickness (Y_s), the downslope and upslope lengths (X_l and X_u), and the maximum height (H)

to eliminate some distracting constants; set

$$X = Sx/H\ , \quad Y = Sy/H\ , \quad h = Hu \quad \text{and} \quad b = B/(HS)\ , \tag{7.41}$$

where H is the dome height at $x = y = 0$. Then,

$$(1 - u_X)^2 + u_Y^2 = \frac{b^2}{u^2}\ . \tag{7.42}$$

Following the convention usually used for nonlinear partial differential equations, we set $p = u_X$ and $q = u_Y$, and write the characteristic equations as:

$$\dot{X} = 2(1-p)\ , \quad \dot{Y} = -2q\ , \quad \dot{u} = 2p(1-p) - 2q^2\ , \quad \text{and} \quad \frac{\dot{p}}{p} = \frac{\dot{q}}{q} = \frac{2b^2}{u^3}\ , \tag{7.43}$$

in which the dot denotes differentiation with respect to the independent variable, τ, the coordinate along each characteristic curve. Suitable initial conditions at $\tau = 0$ are $u = 1$ at $X = Y = 0$, together with parameterized conditions for p and q that satisfy (7.40) at $u = 1$. Two relations follow straightforwardly from the characteristic equations:

$$q = ap \quad \text{and} \quad aX - Y = 2a\tau\ , \tag{7.44}$$

where a is a constant of integration that parameterizes the initial data. We use the second relation of (7.44) to eliminate $\tau = (aX - Y)/2a$. Two further integrals then provide the implicit solution,

$$X = -\int_u^1 \frac{[1-p(\hat{u})]\mathrm{d}\hat{u}}{p(\hat{u})[1-p(\hat{u})(1+a^2)]}\ , \quad Y = a\int_u^1 \frac{\mathrm{d}\hat{u}}{[1-p(\hat{u})(1+a^2)]}\ , \tag{7.45}$$

in which we can exploit the original equation (7.42) to write

$$p(u) = \frac{u \pm \sqrt{b^2(1+a^2) - u^2a^2}}{u(1+a^2)}\ , \tag{7.46}$$

The ambiguity in the construction of $p(u)$ arises because there are two possible solutions for $u(X, Y)$, one upslope and the other downslope of a special curve on the $(X, Y)-$plane. The functions $\Phi(u, a)$ and $\Psi(u, a)$ have analytical, though convoluted, expressions that we shall not burden the reader with.

Explicit solutions follow for $a = 0$ and $a \gg 1$: For $a = 0$, $Y = 0$ and

$$X = \begin{cases} u - 1 + b\log[(u-b)/(1-b)], & X > 0 \\ u - 1 - b\log[(u+b)/(1+b)], & X < 0, \end{cases} \tag{7.47}$$

as in [15] (see also Chap. 6 and [17]). For $a \gg 1$,

$$X = -1 + u - \frac{b}{2}\log\left[\frac{(b-1)(b+u)}{(b+1)(b-u)}\right] \tag{7.48}$$

and

$$Y = \pm\left(\sqrt{b^2 - u^2} - \sqrt{b^2 - 1}\right)\ . \tag{7.49}$$

This second second curve is the junction dividing the two pieces of the solution for $u(X, Y)$.

Sample solutions are shown in Fig. 7.12. As $b \to 1$, the domes are increasingly slumped ($b \propto S^{-1}$, so a decrease in b corresponds to an increase of the slope). The limiting solution for $b \to 1$ is shown in Fig. 7.13. The solution does not work if $b < 1$, indicating that the dome is no longer able to support itself against gravity.

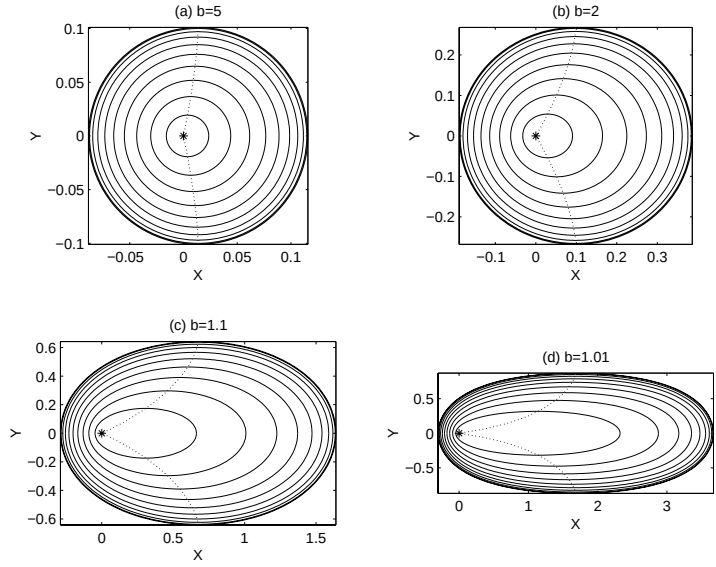

Fig. 7.12. Contours of constant height for yield-stress dominated domes on sloping planes. The dotted curves show the junction between the two parts of the solution

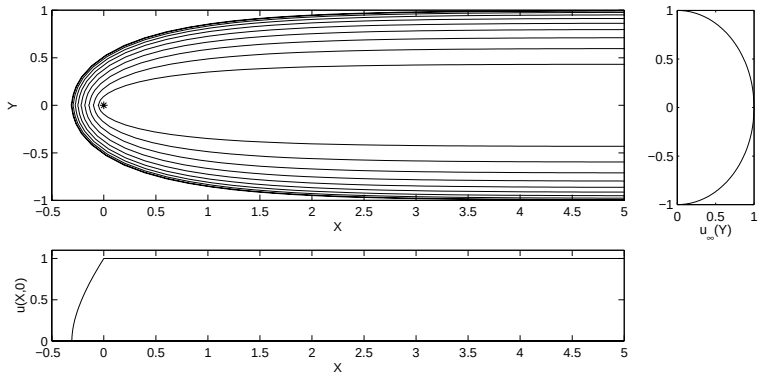

Fig. 7.13. Contours of constant height for the limiting shape as $b \to 1$. Also shown is the thickness profile along the $Y = 0$ axis, given by $u = 1$ for $X > 0$ and the second relation of (7.47), and the thickness profile in Y far downstream ($X \gg 1$), which is a semicircle

7.4.3 Streams and Hulme's Solution

When the slope is larger, the fluid flows downhill and forms a coherent stream rather than a slumping dome. Such streams are often observed for basaltic lavas, and, aside from explosive eruptions, are one of the most pictured volcanic phenomena. Such observations prompted Hulme to write down an approximate solution for one-dimensional flow down an inclined plane [2]. Argued more from plausibility than mathematical deduction, Hulme's model assumes that the stream is composed of a central flowing core flanked by stationary "levees", as illustrated in Fig. 7.14; the flow is purely downhill, and there is no variation in the downslope direction. By assuming that the levees were composed of fluid that naturally came to rest as the flow settled to its asymptotic state, Hulme further argued that the levees should be supported by stresses that were precisely at the yield value. This leads to the important conclusion that one can use observations of the shape of the levee to estimate the yield stress, a fact frequently exploited by volcanologists. However, Hulme's solution has lately been criticized [18], and so we briefly consider its merits.

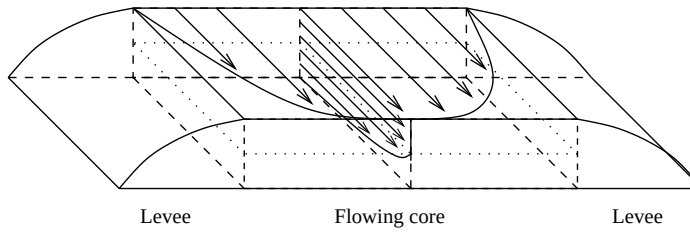

Fig. 7.14. Sketch of Hulme's solution for flow down an inclined plane

Because thin-layer theory is significantly simpler than the governing equations, one can easily look for solutions of the model that correspond to Hulme's. If we insist that the flow is purely downhill and varies only with y, then one concludes that

$$\mathcal{V} = h_y = 0 \,, \quad h = 1 \,, \quad \eta = 1 - \frac{B}{S} \quad \text{and} \quad s = S \,, \tag{7.50}$$

in regions where the fluid yields. That is, a uniform flow. In the levee, on the other hand, the fluid is on the brink of yielding, which implies that $\eta = 0$, or

$$B = h\sqrt{S^2 + h_y^2} \geq SH_l \,, \tag{7.51}$$

where H_l is the maximal thickness of the levee. Unless $H_l < 1$ (and the levee is shallower than the core), this contradicts the flowing solution which requires that $\eta = 1 - B/S > 0$. In other words, one cannot connect the central flowing channel with the stationary levee. This difficulty is not simply a problem with

thin-layer theory – even if one begins from the governing fluid equations, Hulme's construction still appears to be impossible for the same reasons.

The problem with Hulme's construction is that it uses a one-dimensional version of the Bingham fluid model, and consequently does not have the correct, two-dimensional yield criterion: Hulme shapes the levee according to Nye's solution, $B = |hh_y|$, which predicts a parabolic profile, rather than (7.51) (which indicates the profile far downstream is semicircular – see Fig. 7.13). In other words, one assumes that the lateral structure of the levee is the same as the shape the fluid would take on a flat plane – the yielding induced by the downstream flow is ignored. When one takes the extra degree of yield into account, one is led to the inescapable conclusion that, if the levees are to remain as thick as the main channel, the shape of the levees forces lateral flow.

A simple demonstration that the downstream flow affects the lateral shape is afforded by the following experiment with kaolin slurry: We allow a corridor of fluid to slump laterally to a static equilibrium on a horizontal plate. We then tilt the plate in the direction of the central axis of the fluid to create a channel flow. As shown in Fig. 7.15, the main effect of the flow is to allow further lateral spreading of the fluid (except near the upper end of the column, where the thickness remains roughly the same, but some of the fluid drains away). Note also the creation of streamwise flow dependence.

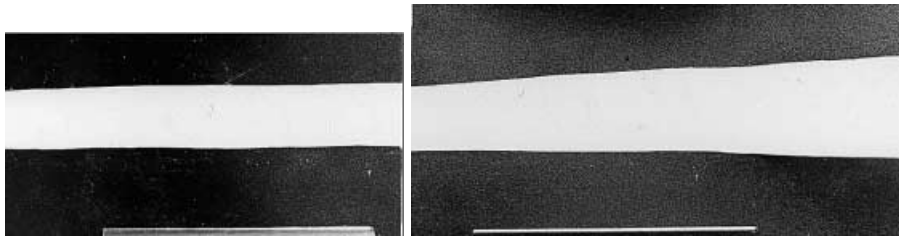

Fig. 7.15. Photographs from an experiment in which a column of viscoplastic fluid (a mixture of water and joint compound) was first allowed to slump to rest on a horizontal plane (first panel). The plane was then tilted at an angle of roughly 25 degrees and as fluid flowed downhill, the column spread laterally and downstream (second panel). The two photographs have the same scale

Because of the theoretical difficulties with Hulme's model, Coussot & Proust suggested another solution taking account of the true yield criterion: Let the flow be independent of time, but not of the streamwise coordinate, x. The thin-layer model equations then become

$$[\mathcal{F}(S - h_x)]_x = [\mathcal{F}h_y]_y \,, \qquad \mathcal{F} = \frac{n\eta h^2 (s\eta h)^{1/n}(1 + 2n - n\eta)}{s(n+1)(2n+1)} \,, \tag{7.52}$$

with η and s as before, and assuming no vertical mass flux (the source of fluid is upstream). Because there is now streamwise variation, the free surface is not

necessarily flat, and Coussot & Proust [18] construct solutions with some correspondence with experiments (see also [19]). Actually, Coussot & Proust do not use the full equation (7.52), but an approximation obtained by neglecting h_x and h_y in comparison with S. Thus s becomes S and we arrive at the parabolic equation $S\mathcal{F}_x = [\mathcal{F}h_y]_y$, with $\mathcal{F}$ as above and $\eta = \mathrm{Max}(1 - B/Sh, 0)$. This approximation cannot be accurate at the edges of the stream where the gradients of $h(x, y)$ diverge, but these regions are also where the thin-layer model breaks down.

The analytical solution pictured in Fig. 7.13 shows similar features to Coussot & Proust's downstream spreading flows. Further numerical computations are shown in Fig. 7.16. In this case, with $B = 0.06$ and $S = 2$, the fluid immediately slumps downhill without forming a dome, and creates a gradually widening stream.

A laboratory illustration of a stream flow is shown in Fig. 7.17. This inclined flow has well-defined levees bordering the flow but also spreads laterally with distance downstream. Similar features can be seen in Osmond & Griffiths's domes (Chap. 6 and [15]). Thus, although Hulme's "solution" is not actually a solution of the equations, the image is not entirely wrong: the stationary levees supported by stresses at the yield value do exist – Hulme's precise construction is invalid because the flow spreads downstream and the levees are not shaped according to Nye's solution. Thus Hulme's image is qualitatively correct, if not quantitatively.

Although the final conclusion is that Hulme's solution is in error, the ramifications in geology regarding estimations of yield stress are probably inconsequential: Rheological measurements of lava are exceptionally difficult because of its extreme temperature, and it is probably fair to say that actual values of the yield stress are not known to within orders of magnitude. Hence, although the correction to the shape of the levee given the slope S will certainly change the inferred value of the yield stress by an order one amount, this is insignificant in comparison to other rheological uncertainty. Osmond & Griffiths [15] discuss further how to infer yield stresses given the proper yield condition.

7.5 Concluding Remarks

The purpose of a thin-layer theory is to reduce the full, governing fluid mechanical equations to a more manageable form. For non-isothermal lava flows, because heat conduction occurs relatively slowly, the thin layer theory remains fairly complicated, as in shallow-ice theories. However, the reduced equations contain all the relevant physics in a concise form, and filter out any complicating, but inessential details. The analogue experiments for isothermal domes show that thin-layer theory is accurate over a wide range of extrusion rates and rheological parameters. Some related experiments, with fluid flowing down an inclined plane (and performed to test similar theory for mud flow), show a comparable degree of agreement [13]. Hence shallow-fluid theory appears to be a useful route to take whilst modelling geophysical viscoplastic fluids.

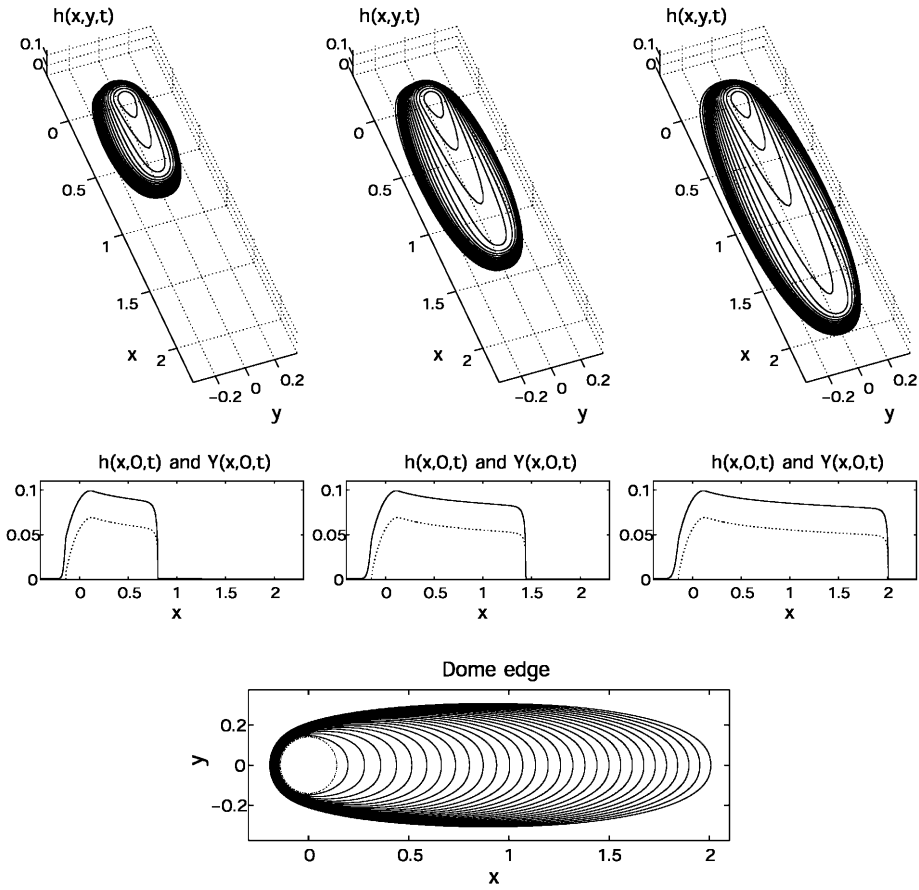

Fig. 7.16. A flow down an inclined planes, computed numerically using the thin-layer model. The top row of pictures show three snapshots of the domes at times 333, 666 and 1000. Directly below are the corresponding height profiles and yield surfaces along the midsection ($y = 0$). The lower panel shows a sequence of curves showing the dome's edge (the curves show the edge every 6.66 time units)

Fig. 7.17. Photographs from an experiment in which viscoplastic fluid (a mixture of water and joint compound) was extruded onto a sloping plane (inclined by roughly 30 degrees). Shown is the final shape after the extrusion was terminated and the fluid allowed to come to rest on the plane

There are several extensions to the theory that must be pursued for a description of lava flows, and the subject is rich with problems to examine. For example, it is essential to solve the non-isothermal problem outlined at the beginning of this article. But there are several other issues that we have not dwelt upon here, such as the detailed mechanics at the edge of the fluid where the flow over-rides the substrate. Notably, the analogue experiments should also be taken further, and theoretical computations should be compared systematically with non-isothermal extrusions.

Beyond the formulation and testing of a shallow-lava theory lies the applications to real geological problems. The shallow-lava theory provides a computationally convenient tool to analyze lava flows in geological settings. For example, one might wish to predict the direction of a lava flow over complex terrain and assess possible hazards. Alternatively, the goal may be to predict which lava domes are most likely to allow the internal build up of hot gas, which could lead to structural failure, explosions and pyroclastic flows (Chap. 8). Of course, we already have some answers to such questions, based on cruder theoretical models (such as approximating the lava as an isothermal viscous fluid) or qualitative arguments (for example, if the lava has a yield stress, a dome can sustain large internal pressures, thus trapping gas within the dome). The real question is whether our more quantitative modelling has any advantage over these simpler arguments, given the uncertainties, idealizations and approximations in the theory. We cannot answer this particular question until we have fully formulated a usable non-isothermal shallow-lava theory, but the hope is that the theory will significantly improve our predictive capabilities, and place the modelling of lava flows on a more solid foundation.

Acknowledgements

The financial support of an EPSRC Advanced Fellowship is gratefully acknowledged by RVC. This work was supported by the National Science Foundation (Grant No. DMS0072521).

References

1. R.W. Griffiths: Ann. Rev. Fluid Mech. **32**, 477 (2000)
2. G. Hulme: Geophys. J. Roy. Astron. Soc. **39**, 361 (1974)
3. S. Blake: 'Viscoplastic models of lava domes'. In: *Lava flows and domes: emplacement mechanisms and hazard implications*, ed. by J.H. Fink, pp. 88–128. IAVCEI Proc. in Volcanology, vol. 2, Springer–Verlag (1990)
4. R.W. Griffiths, J.H. Fink: J. Fluid Mech. **252**, 667 (1993)
5. M.V. Stasiuk, C. Jaupart, R.S.J. Sparks: Geology **21**, 335 (1993)
6. R.W. Griffiths, J.H. Fink: J. Fluid Mech. **347**, 13 (1997)
7. B. Reisfeild, S.G. Bankohh, S.H. Davis: J. Appl. Phys. **70**, 5258 and 5267 (1991)
8. A. Neri: J. Volcan. Geotherm. Res. **81**, 215 (1998)
9. N.J. Balmforth, R.V. Craster: J. Fluid Mech. **422**, 225 (2000)
10. N.J. Balmforth, R.V. Craster: J. Non-Newtonian Fluid Mech. **84**, 65 (1999)

11. H.E. Huppert: J. Fluid Mech. **121**, 43 (1982)
12. J.F. Nye: J. Glaciology **2**, 82 (1952)
13. K.F. Liu, C.C. Mei: J. Fluid Mech. **207**, 505 (1989)
14. I.N. Sneddon: *Elements of Partial Differential Equations* (McGraw–Hill 1957)
15. D.I. Osmond, R. Griffiths: J. Fluid Mech. (in press 2001)
16. J.G. Blom, R.A. Trompert, J.G. Verwer: ACM Trans. Math. Software **22**, 302 (1996)
17. P. Coussot, S. Proust, C. Ancey: J. Non-Newtonian Fluid Mech. **66**, 55 (1996)
18. P. Coussot, S. Proust: J. Geophys. Res. **101**, 25217 (1996)
19. S.D.R. Wilson, S.L. Burgess: J. Non-Newtonian Fluid Mech. **79**, 77 (1998)